Identifying decadal trends in deweathered concentrations of criteria air pollutants in Canadian urban atmospheres with machine learning approaches

Xiaohong Yao[1,*], Leiming Zhang[2,*]

[1] Key Laboratory of Marine Environment and Ecology (MoE), Frontiers Science Center for Deep Ocean Multispheres and Earth System, and Sanya Oceanographic Institution, Ocean University of China, Qingdao 266100, China

[2]Air Quality Research Division, Science and Technology Branch, Environment and Climate Change Canada, Toronto, M3H 5T4, Canada

*Corresponds to: xhyao@ouc.edu.cn, leiming.zhang@ec.gc.ca

Abstract. This study investigates long-term trends of criteria air pollutants, including NO_2, CO, SO_2, O_3 and $PM_{2.5}$, and O_x (=NO_2+O_3) measured in ten Canadian cities during the last two to three decades and associated driving forces in terms of emission reductions, perturbations due to varying weather conditions and large-scale wildfires, and changes in O_3 sources and sinks. Two machine learning methods, the random forest algorithm and boosted regression trees, were used to extract deweathered mixing ratios (or mass concentrations) of the pollutants. The Mann-Kendall trend test of the deweathered and original annual average concentrations of the pollutants showed that, on the time scale of 20 years or longer, perturbation due to varying weather conditions on the decade trends of the pollutants are minimal (within ±2%) in about 70% of the studied cases, although it might be larger (but at most 16%) in the remaining cases. NO_2, CO and SO_2 showed decreasing trends in the last two to three decades in all the cities except CO in Montreal. O_3 showed increasing trends in all the cities except Halifax, mainly due to weakened titration reaction between O_3 and NO. O_x, however, showed decreasing trends in all the cities except Victoria because the increase in O_3 is much less than the decrease in NO_2. In three of the five eastern Canadian cities, emission reductions dominated the decreasing trends in $PM_{2.5}$, but no significant trends

in $PM_{2.5}$ were observed in the other two cites. In five western Canadian cities, increasing or no significant trends in $PM_{2.5}$ were observed, likely due to unpredictable large-scale wildfires overwhelming or balancing the impacts of emission reductions on $PM_{2.5}$. In addition, despite improving air quality during the last two decades in most cities, air quality health index of above 10 (representing very high-risk condition) still occasionally occurred after 2010 in western Canadian cities because of the increased large-scale wildfires.

Keywords: Atmospheric pollutants, trend analysis, machine learning, emission reduction, wildfire emission

1 Introduction

Criteria air pollutants can harm human health and the natural environment. According to Health Impacts of Air pollution in Canada 2021 Report (Heath Canada, 2021), it is estimated that air pollution of NO_2, O_3 and $PM_{2.5}$ caused 15,300 deaths per year, corresponding to 42 deaths per 100,000 population in Canada in 2016. To protect human health and the environment, the Canadian Council of Ministers of the Environment (CCME) developed the Canadian Ambient Air Quality Standards (CAAQS) for $PM_{2.5}$, O_3, SO_2 and NO_2. CAAQS are supported by four colour-coded management levels with each management level being determined by the amount of a pollutant within an air zone, from which recommendations on air quality management actions are provided. Following this standard, multiphase mitigation measures have been implemented to largely reduce anthropogenic air pollutant emissions in recent decades (ECCC, 2021). Air quality in Canadian urban atmospheres well meets CAAQS in recent years, as reported in Air Quality - Canadian Environmental Sustainability Indictors (ECCC, 2023).

Nevertheless, the World Health Organization (WHO, 2021) updated the global air quality guidelines (AQG) on NO_2, SO_2, CO, O_3 and $PM_{2.5}$ in 2021, based on

accumulated strong evidence that air pollution can affect public health even at very low concentrations. In the WHO 2021 AQG, NO_2 annual average concentration is set as 10 μg m^{-3}, equivalent to ~ 5 ppb at annual average temperatures of 6-10 °C across Canada, annual average and 24-hour average $PM_{2.5}$ concentrations are set as 5 μg m^{-3} and 15 μg m^{-3}, respectively, and peak season mean 8-hr O_3 concentration is set as 60 μg m^{-3}. An urgent issue for all areas of the world is to overcome challenges to further lower ambient NO_2, O_3 and $PM_{2.5}$ concentrations in order to meet the WHO 2021 AQG (Dabek-Zlotorzynska et al., 2019; Griffin et al., 2020; Xu et al., 2019; Jeong et al., 2020; Al-Abadleh et al., 2021; Wang et al., 2021; Zhang et al., 2022; Bowdalo et al., 2022).

In search of the most efficient mitigation measures for criteria pollutants, the effectiveness of existing measures on air pollution reduction needs to be first examined. For this purpose, long-term trends in concentrations of the criteria air pollutants need to be quantified and the driving forces of the trends, besides anthropogenic emission reductions, should be identified. Several studies have investigated the decadal trends of some criteria pollutants in Canada in the past decade. For example, Chan and Vet (2010) reported upward trends in O_3 mixing ratio from 1997-2006 at dozens of sites in Canada. Xu et al. (2019) and Zhang et al. (2022) also found increasing trends in O_3 mixing ratio from 1996-2016 at multiple sites in Windsor, Ontario, which was attributed to the reduced titration effect of NO with O_3. They also reported that the 95^{th} percentile O_3 mixing ratio exhibited a decreasing trend and attributed the decrease to anthropogenic emission reductions. Mitchell et al. (2021) reported that the 99^{th} percentile O_3 mixing ratios exhibited a decreasing trend from 2000-2018 at urban and regional sites in Nova Scotia, but such a trend was not found for low-moderate percentile O_3 mixing ratios. Bari and Kindzierski (2016) found no significant trends in $PM_{2.5}$ mass concentration, although decreasing trends in organic carbon and elemental carbon from 2007-2014 in Edmonton. Jeong et al. (2020) reported 34% decrease in $PM_{2.5}$ mass concentration from 2004-2017 in Toronto and attributed the decrease to the reduced coal-fired power plants emissions. Wang et al. (2022a) reported significant decreasing trends in organic and

elemental carbon in $PM_{2.5}$ from 2003-2019 at seven urban sites in Canada. Studies on other criteria pollutants are very limited (Feng et al., 2020; Jeong et al.; 2020).

O_3 mixing ratios, especially at high levels, are strongly affected by meteorological conditions, and thus, trends on the decadal scale can be perturbed by varying weather conditions from year to year (Simon et al., 2015; Xing et al., 2015; Ma et al., 2021; Lin et al., 2022). Inter-annual variations of weather conditions also have strong impact on the decadal trends of other criteria pollutants (Lin et al., 2022). Air quality models are useful tools to analyze emission-driven air quality trends and meteorological impacts (Foley et al., 2015; Astitha et al., 2017; Vu et al., 2019), but most modeling results suffer from large uncertainties which could exceed changes in annual means of simulated pollutant concentrations. Machine learning techniques such as the random forest (RF) algorithm and boosted regression trees (BRTs) have been demonstrated to be a powerful tool to decouple impacts of emission changes and perturbations from varying weather and/or meteorological conditions, enabling the derivation of deweathered trends in air pollutants concentrations (Grange et al., 2018; Grange and Carslaw, 2019; Ma et al., 2021; Mallet, 2021; Shi and Brasseur, 2020; Wang et al., 2020; Munir et al., 2021; Lovric et al., 2021; Hou et al., 2022; Lin et al., 2022). The advantages and limitations of RF algorithm and BRTs have been described in detail in earlier studies (Grange et al., 2018; Grange and Carslaw, 2019). Briefly, BRTs method is fast to train and make prediction, but suffers heavily from overfitting, which may result in unreliable predictions. RF method can control the overfitting, but yields a poor prediction for outliers in large percentiles. Thus, using two methods with different strengths and weaknesses, although their predictions are similar in many ways, can constrain methodology uncertainties and better evaluate perturbations due to varying weather conditions than using only one method, as has been demonstrated in our earlier study (Lin et al., 2022).

This study attempts to deduct the perturbations due to varying weather conditions on

the observed mixing ratios (or mass concentrations) of some criteria air pollutants in Canada during the past two to three decades and thereby investigates their emission-driven trends. We used the RF algorithm and BRTs to generate the deweathered mixing ratios (or concentrations) of NO_2, SO_2, CO, O_3, O_x and $PM_{2.5}$ during the past decades in ten cities equally distributed in eastern and western Canada. Considering that the machine learning methods may suffer from the weakness in accurately predicting large percentile concentrations of the studied criteria air pollutants, we also applied our previously developed identical-percentile autocorrelation analysis method to better quantify the perturbations due to extreme events such as large-scale wildfires on large percentile $PM_{2.5}$ concentrations (Yao and Zhang, 2020; Lin et al., 2022). The Mann-Kendall (M-K) trend test was then employed to resolve the trends in the deweathered mixing ratios (or mass concentrations). Pearson correlation analysis was further conducted for the deweathered and original mixing ratios (or mass concentrations) of the air pollutants against the corresponding provincial-level emissions. City-level emissions were used in the analysis in cases with large differences between air pollutant concentrations and provincial-level emissions. In addition, the Air Quality Heath Index (AQHI, https://weather.gc.ca/airquality/pages/index_e.html), a health protection tool designed in Canada to advise the public to adjust outdoor activities based on air pollution levels, was also analyzed with particular attention to the trends with AQHI being above 7 and 10, respectively. This study provides a thorough assessment of the emission-driven trends in the studied criteria pollutants on the time scale of two to three decades across Canadian urban atmospheres, knowledge from which is much needed in developing future emission control policies of the concerned pollutants.

2 Methodology

2.1 Monitoring sites and data sources

Ten major cities, including five in eastern Canada (Halifax, Quebec City, Montreal, Toronto and Hamilton) and five in western Canada (Winnipeg, Calgary, Edmonton, Vancouver and Victoria), from the National Air Pollution Surveillance (NAPS) program

are selected for investigating decadal trends of the monitored criteria pollutants (Table S1). The NAPS program has long-term air quality data of a uniform standard across Canada (Dabek-Zlotorzynska et al., 2011, 2019; Jeong et al., 2020; Yao and Zhang, 2020; Wang et al., 2021, 2022a). The NAPS program includes both continuous and time-integrated measurements of gaseous and particulate air pollutants. Continuous data are available as hourly concentrations and are quality-assured as specified in the Ambient Air Monitoring and Quality Assurance/Quality Control Guidelines (https://open.canada.ca/data/en/dataset/1b36a356-defd-4813-acea-47bc3abd859b).

Multiple monitoring sites exist in most cities, but only one urban background site was selected in each city mentioned above based on the following criteria: with the most complete dataset of the five selected criteria pollutants (NO_2, CO, SO_2, O_3 and $PM_{2.5}$), with the longest data record, and with valid data in each year (Table S1). In cases with a data gap longer than a year, e.g., in Quebec City, Halifax and Calgary, data at a nearby urban background site (within 1 km) were then used to fill the gap. If no site within 1 km is available, then the data gap is left unfilled. SO_2, CO, NO_x and $PM_{2.5}$ emission data at the provincial level in Canada are obtained from https://www.canada.ca/en/environment-climate-change/services/environmental-indicators/air-pollutant-emissions.html. City-level air pollutant emissions from various registered facilities since 2002 were obtained from https://www.canada.ca/en/services/environment/pollution-waste-management/national-pollutant-release-inventory.html.

Besides the monitored criteria pollutants described above, AQHI is also calculated in this study at three-hour resolution using the following formula (Stieb et al., 2008; To et al., 2013):

AQHI = $(100/10.4) * ([(e^{0.000537*O3}-1) + (e^{0.000871*NO2}-1) + (e^{0.000537*PM2.5}-1)]$, in which O_3 and NO_2 represent their respective three-hour average original mixing ratios (in ppb) and $PM_{2.5}$ represents its three-hour average original concentration (in µg m^{-3}). The

calculated AQHI is rounded to the nearest positive integer. AQHI between 1-3 represents excellent air quality that is safe for outdoor activities. Outdoor activities may be reduced at AQHI between 4-6 for certain population with some health issues. AQHI between 7-10 and >10 correspond to high and very high health risk conditions, respectively. Note that four alternative AQHI-Plus amendments have been proposed for wildfire seasons and the AQHI-Plus values are always larger than the corresponding AQHI values (Yao et al., 2020). One of AQHI-Plus amendments has been implemented in late 2016 in British Columbia. The AQHI-Plus amendments are not used in this study since it is not implemented across the whole Canada.

2.2 Statistical analysis

In this study, two popular machine learning packages, including the “rmweather” R package (Grange et al., 2018) and the “deweather” R package (Carslaw and Ropkins, 2012; Carslaw and Taylor, 2009), were used to perform the RF algorithm and the BRTs, respectively. Besides the monitored hourly average mixing ratio (or mass concentration) of a pollutant, temporal variables (hour, day, weekday, week and month) and meteorological parameters (wind speed, wind direction, ambient temperature, relative humidity and dew point) are also needed as additional independent inputs to the machining learning process. The hourly meteorological data were obtained from the meteorological observational station at a nearby airport in each city, which are accessible from the NOAA Integrated Surface Database (ISD) by using the “worldmet” R package (Carslaw, 2021). The meteorological data from the nearest airport in every city should reflect synoptic weather conditions, which have been used in existing machine learning studies (Vu et al., 2019; Mallet, 2020; Wang et al., 2020; Dai et al., 2021; Ma et al., 2021). Additional meteorological parameters such as boundary layer height, total cloud cover, surface net solar radiation, surface pressure, total precipitation and air mass clusters have also been used in some studies to improve the performance of the machine learning methods (Hou et al., 2022; Shi et al., 2021; Lin et al., 2022). These additional meteorological parameters were not included in the present study, but

could be included in future analyses. Nevertheless, good performance can still be achieved in the present study mainly because of multi-decade length of the datasets, as demonstrated by an example shown in Fig. 1. Note that the inputs for the two packages were randomly divided into two groups and the user cannot control the division, i.e., the training dataset that used 80% of the data and a testing dataset that used the remaining 20%. Thus, the testing datasets were different between the RF algorithm and the BRTs. Note that all input parameters and output variables, i.e., the predicted hourly average mixing ratio (or mass concentration) of a pollutant, for testing were the same as those used for learning. Moreover, the training and testing were conducted for every pollutant at every site.

Five statistical metrics, including coefficient of determination (R^2), root mean square error (RMSE), mean bias (MB), mean fractional bias (MFB) and mean fractional error (MFE), were calculated to evaluate the performance of the two machine learning methods. In the literature, criteria and goal values have not been set for the statistical metrics for the purpose of evaluating machine learning prediction performance. Alternatively, the criteria and goal values for MFE and MFB proposed by USEPA are adopted here, which are MFE≤75% and MFB≤±60% for the criteria value and MFE≤50% and MFB≤±30% for the goal value (USEPA, 2007).

Fig. 1 shows predictions against observations of NO_2 mixing ratio in Halifax using the testing datasets during 1996-2017, as an example for evaluating the performance of the two machine learning methods (P value <0.01 for all the correlation). MFB and MFE values were far below their respective goal values for both RF algorithm and BRTs set by USEPA. R^2 and RMSE were 0.86 and 5.1, respectively, for both methods. MB is -0.04 for RF algorithm and 0.1 for BRTs. The values of these metrics indicated that the predictions well reproduced the observations. However, the two machine learning methods overall underpredicted NO_2 mixing ratios to a small extent based on the regression lines slightly below the 1:1 line. The underestimation was mainly due to

sporadic large values in the measurement of NO_2 mixing ratio, which did not provide sufficient samples for the machine learning methods to learn and yield good predictions. For all the pollutants in all the cities investigated in this study, the machine learning predictions generally met the goal values set by USEPA, except for $PM_{2.5}$ in some western Canadian cities such as Calgary and Edmonton with the predictions only meeting criteria values because of the perturbation from large-scale wildfires.

Following the approach described in earlier studies (Hou et al., 2022; Lin et al., 2022), the two machine learning methods were run for 1000 times with meteorological variables randomly resampled from the entire datasets during the study period. The average model prediction from the 1000 model runs represents the meteorologically normalized pollutant concentration at a particular time. We also tested averaging 2000 and 3000 model predictions, which produced consistent results with those of using 1000 model predictions. Thus, averaging 1000 model predictions was used for meteorological normalization in this study.

As mentioned above, the machine learning methods suffer from the weakness in accurately predicting high concentration values in large percentiles. We thus applied the identical-percentile autocorrelation analysis method developed in our previous study to quantify the perturbations due to extreme events such as large-scale wildfires on the large percentile concentration values (Yao and Zhang, 2020; Lin et al., 2022). This method has five steps for data processing and analysis. The first step is to construct a long-term average data series at hourly resolution covering 365 days by averaging the corresponding hourly data from all the years of the study period. The second step is to pair a data series at any given year to the long-term average data series, and if there were any data gaps (missing hours) in the former data series, data for these hours in the latter series were also removed so that the two data series have exactly the same size. The third step is to rearrange all the hourly data from the smallest to the largest value in each of the data series generated in step 2, and then conduct correlation analysis

between the pair of data series. Inflection points in the large and small percentile zone were first visibly identified/guessed, and referenced as upper and lower inflection points, respectively. The pair of data between the lower and upper inflection points were correlated repeatedly by varying values of the two inflection points in search for highest R^2 values. The fourth step is to predict the large percentile values exceeding the upper inflection point using the regression equation with the highest R^2 generated in step 3. The final step is to obtain the perturbations due to extreme events on the large percentile concentrations by subtracting the observed values from the predicted values.

Fig. 2 shows three examples calculating the perturbations due to varying weather conditions and large-scale wildfires on the large percentile concentrations of $PM_{2.5}$ in 1998, 1999 and 2019 in Edmonton. Large-scale wildfires occurred in 1998 and 2019 (Fig. S1), but no record in 1999. In 1998, data points outside the 4.5^{th}-94^{th} percentile range were screened out through steps 1-3, and the remaining data points were used to obtain a regression equation, which shows $[PM_{2.5}]_{data\ in\ 1998} = [PM_{2.5}]_{long\text{-}term\ average} * 3.9\text{-}18$ (R^2=0.96, P<0.01) (Fig. 2a). $[PM_{2.5}]_{data\ in\ 1998}$ and $[PM_{2.5}]_{long\text{-}term\ average}$ represent the same identical percentile values of $PM_{2.5}$ in re-organized data series of 1998 and the long-term average through steps 1-3, respectively. The similar definition is applicable for $[PM_{2.5}]_{data\ in\ 1999}$ and $[PM_{2.5}]_{data\ in\ 2019}$ presented below. In 1999, data points within the 4.5^{th}-99.7^{th} percentile range resulted in a regression equation of $[PM_{2.5}]_{data\ in\ 1999} = [PM_{2.5}]_{long\text{-}term\ average} * 3.1\text{-}15$ (R^2=0.97, P<0.01) (Fig. 2c). In 2019, data points within the 5.4^{th}–96^{th} percentile range resulted in $[PM_{2.5}]_{data\ in\ 2019} = [PM_{2.5}]_{long\text{-}term\ average} * 2.2\text{-}12$ (R^2=0.94, P<0.01) (Fig. 2e). Note that step 3 is critical to obtain these excellent correlations (Fig. 2a, 2c and 2e) as compared with those absent of step 3 (Fig. 2b, 2d and 2f).

The perturbation due to the extreme weather conditions or the extreme events on the 100^{th} percentile $PM_{2.5}$ value, i.e., the maximum value in this study, at a particular year (y) can be calculated as:

$[PM_{2.5}]_{perturbation\ at\ 100th,y} = [PM_{2.5}]_{predicted\ at\ 100th,y} - [PM_{2.5}]_{observed\ at\ 100th,y}$

$[PM_{2.5}]_{predicted\ at\ 100th,y} = [PM_{2.5}]_{long\text{-}term\ average\ at\ 100th} * k_y + b_y$

where $[PM_{2.5}]_{observed\ at\ 100th,y}$ represents the 100^{th} percentile $PM_{2.5}$ value observed in y year, and k_y and b_y represent the slope and intercept, respectively, of the regression equation with the highest R^2 in the y year generated through steps 1-3. Similarly, the perturbation inherent from the large percentile values from the final upper inflection point (m^{th}) to 100^{th} percentile in a particular year can be calculated as:

$[PM_{2.5}]_{perturbation\ at\ \geq mth,\ y} = [PM_{2.5}]_{predicted\ at\ \geq mth,\ y} - [PM_{2.5}]_{observed\ at\ \geq mth,\ y,}$

$[PM_{2.5}]_{predicted\ at\ mth,y} = [PM_{2.5}]_{long\text{-}term\ average\ at\ mth} * k_y + b_y$

The calculated values from $[PM_{2.5}]_{perturbation\ at\ \geq mth,y}$ to $[PM_{2.5}]_{perturbation\ at\ 100th,y}$ in the y year were averaged as $[PM_{2.5}]_{perturbation\ average,y}$. The perturbation contribution to the corresponding original annual average equals to $[PM_{2.5}]_{perturbation\ average,y}*(1\text{-}m\%)$ in y year, and the values were 3.0 μg m^{-3} in 1998, 0.2 μg m^{-3} in 1999 and 1.7 μg m^{-3} in 2019 in Edmonton, corresponding to strong, minimal and moderate perturbations, respectively, from large wildfires.

The M-K trend test is a non-parametric test applicable to any type of data distribution and is employed to resolve the trends in the time series of the deweathered and original annual average concentration of each pollutant. Qualitative trends revolved by the M-K trend test include 1) an increasing or decreasing trend with a P value of <0.05, and 2) no significant trend including a probably increasing or decreasing trend, a stable trend, and a no-trend with all the other conditions (Aziz et al., 2003; Kampata et al., 2008; Yao and Zhang, 2020). The extracted trends and associated driving factors are discussed in detail below.

3. Results

3.1 Trends in deweathered and original NO_2 mixing ratios

Fig. 3a and 3b show decadal variations in the original annual averages of NO_2 mixing ratios in the ten Canadian cities. The BRTs-deweathered and RF-deweathered hourly

averages of NO_2 mixing ratios are shown in Fig S2, in which the deweathered results were also interpreted in terms of increased or reduced emissions of NO_x. The decadal trends resulted from annual averages of BRTs-deweathered, RF-deweathered and original NO_2 mixing ratios are listed in Table 1.

The deweathered and original annual average NO_2 mixing ratios in any of the 10 cities both showed consistent decreasing trends in the last 2-3 decades ($P<0.05$ through M-K trend test). The BRTs-deweathered and RF-deweathered annual averages highly correlated with the original values with $R^2>0.95$ and $P<0.01$ (Table 1). The slopes of zero-intercept regression equations between the deweathered and original annual average NO_2 mixing ratios were mostly within 0.98-1.04, indicating ≤4% differences between the deweathered and original annual values. These results indicated that the perturbation due to varying weather conditions only exerted minor influences on the original annual averages. The only exception is the RF-deweathered annual averages in Halifax (with a slope of 1.08); however, this may not suggest that the perturbation due to varying weather conditions was as high as 8% since the BRTs-deweathered annual averages in the same city showed a slope of only 1.03, indicating that the uncertainties in the slope associated with the RF-deweathered averages can be as large as 5% (8% minus 3%) because of its poor prediction for large outlier values.

The annual decreasing rates in the deweathered and original NO_2 mixing ratios in the studied cities varied from 0.31 to 0.74 ppb year $^{-1}$, and the overall percentage decreases ranged from 37% to 62% during the last two to three decades (Table 1). Our results suggested that varying weather conditions likely played a negligible role in the annual decreasing rates of NO_2 mixing ratio in two eastern (Montreal and Hamilton) and four western (Winnipeg, Calgary, Vancouver and Victoria) Canadian cities, as can be seen from the very close annual decreasing rates between the deweathered and original annual average mixing ratios, despite methodology uncertainties in generating deweathered mixing ratios as mentioned above. In the remaining four cities, the annual

decreasing rates were always larger in the original than the deweathered annual average NO_2 mixing ratio, with the largest differences in Toronto (0.07-0.10 ppb $year^{-1}$), followed by Halifax (0.06-0.10 ppb $year^{-1}$), Edmonton (0.06-0.08 ppb $year^{-1}$) and Quebec City (0.02-0.07 ppb $year^{-1}$), suggesting that varying weather conditions contributed appreciably to the annual decreasing rate. The annual decreasing rates were highly city-dependent, but there were no significant differences between eastern and western cities ($P>0.05$). With continuously decreasing NO_2 mixing ratios in the last decades (Fig. 3), annual average NO_2 fell to below 10 ppb by 2019 in half of the studied cities (Halifax, Montreal, Quebec City, Winnipeg and Victoria), meeting the WHO 2021 guideline. Additional efforts are still needed to lower the NO_2 level in the rest of the cities, especially in Toronto and Edmonton in which annual average NO_2 were still as high as 15 ppb in 2019.

NO_2 in urban atmospheres were mainly formed by the rapid titration reaction of NO with O_3, with NO largely released from anthropogenic emissions, especially the transport sector (Pappin et al., 2016; Casquero-Vera et al., 2019; Dabek-Zlotorzynska et al., 2019; Feng et a., 2020; Griffin et al., 2020; Al-Abadleh et al., 2021). The correlations between the annual average NO_2 mixing ratios and corresponding provincial NO_x emissions were thereby analyzed below (Table 1). Note that the on-line air pollutant emission inventory in Canada reports the emissions since 1990 (ECCC, 2021) so the correlation analysis only covers the period of 1990-2019. Strong correlations (R^2=0.82-0.98) were obtained in all of the five eastern Canadian cities. The overall decreasing percentages of the deweathered and original NO_2 mixing ratios in Halifax and Quebec City were roughly the same as that of the provincial grand total NO_x emissions and transportation NO_x emissions, but in Montreal, Toronto and Hamilton the former decreasing percentages were smaller than the latter ones. In contrast, the overall decreasing percentages in NO_2 mixing ratio in the five western Canadian cities were substantially larger than the corresponding decreasing percentages of the provincial grand total NO_x emissions and transportation NO_x emissions, and the

correlation (R^2=0.54-0.94) between NO_2 mixing ratio and provincial emission were not as good as those in eastern cities. The extreme case occurred in Calgary, where NO_2 mixing ratio decreased by 31-33% during 1990-2007 when the grand total NO_x emissions and transportation NO_x emissions in Alberta increased by 11% and 5%, respectively, noting that a much short period of data were used in this than other cities. The city-level NO_x emissions recorded from various facilities in Calgary increased from 68 tons in 2002 to 262 tons in 2007 (Table S2), which cannot explain the decrease in NO_2 mixing ratios.

3.2 Trends in deweathered and original mixing ratios of CO and SO_2

As mentioned earlier, CO and SO_2 in Canadian cities well meet the CAAQS in recent years. The original annual average mixing ratios of CO and SO_2 in the ten cities generally met the WHO 2021 air quality guidelines in the last decade, except SO_2 in Hamilton (Fig. S4). Thus, the analysis results on deweathered and original mixing ratios of SO_2 and CO in the nine cities and CO in Hamilton were only briefly summarized below, leaving SO_2 in Hamilton to be discussed separately.

The annual averages of the deweathered CO mixing ratios were reasonably consistent with the original annual averages in five cities, e.g., the slopes of the deweathered mixing ratios against the original ones varied from 0.97 to 1.03 in Montreal, Hamilton, Winnipeg, Edmonton, Vancouver and Victoria, although somewhat large differences between the deweathered and original mixing rations were seen in Quebec City with a slope of 1.12 (RF vs. Origin) and Toronto with a slope of 0.92 (BRTs vs. Origin). The original and deweathered annual averages of CO decreased by ≥82% in the last 2-3 decades in six cities, including Halifax (90-92%), Calgary (90-91%), Winnipeg (84-88%), Edmonton (86-86%), Toronto (83-86%) and Vancouver (82-83%) (Table S3), followed by 66-70% in Hamilton and less than 60% in Quebec City (56-58%) and Victoria (57-59%). Large percentage decreases in baseline CO mixing ratios across North America were reported before (Zhou et al., 2017). The deweathered and original

annual averages of CO mixing ratio significantly correlated with the corresponding provincial grand total emissions and transportation emissions of CO (R^2 =0.68-0.96, P<0.01) in these nine cities. The overall percentage decreases in CO mixing ratio in Quebec City and Victoria were approximately the same as those in the corresponding provincial transportation emissions of CO; however, the former percentage decreases were evidently larger than the latter ones in the other seven cities mentioned above. In Montreal, no significant trends were obtained in the deweathered and original CO mixing ratios during 1995-2010 (P>0.05), despite that the provincial total CO emissions and transportation CO emissions decreased by 37% and 53%, respectively, during the same period.

The deweathered and original annual average mixing ratios of SO_2 decreased by 89-97% in the last 2-3 decades in four cities, including Winnipeg (95-97%), Vancouver (90-95%), Toronto (89-95%) and Halifax (90-93%), followed by 79-86% in Montreal, 78-85% in Quebec City, 73-82% in Victoria, 62-64% in Calgary and 52-55% in Edmonton (Table S4). Large percentage decreases in SO_2 mixing ratio have been reported in rural atmospheres across North America during the last 2-3 decades (Xing et al., 2015; Feng et al., 2020). Since 1990, the overall decreasing percentages in SO_2 mixing ratio in Halifax, Toronto, Calgary and Vancouver were evidently larger than those of the corresponding provincial grand total SO_2 emissions. In Montreal, Quebec City, Winnipeg and Edmonton, the percentage decreases in SO_2 mixing ratio were close to those in the corresponding provincial grand total SO_2 emissions during the same periods. Although SO_2 mixing ratio in Victoria decreased by 73-82% during 1999-2019, the corresponding provincial grand total SO_2 emission did not decrease much during the same period. However, the city-level SO_2 emissions from registered facilities in Victoria decreased from 217 tons in 2002 to near zero in 2019 (Table S2), supporting the decreases in SO_2 mixing ratios. Note that the differences between the two deweathered mixing ratios of SO_2 were enlarged to some extent in comparison with other pollutants, e.g., with the differences being 10-12% for SO_2, but only 2-5% for

NO_2 (as presented above), in Montreal, Toronto and Winnipeg. The increased uncertainties led to the difference between the RF-deweathered and original SO_2 mixing ratios being up to 16% in Winnipeg, based on the slope of 1.16 listed in Table S4. The difference between the BRTs-deweathered and original SO_2 mixing ratios was, however, only 4%, suggesting that the perturbation due to varying weather conditions might be within 4%-16%. Again, the RF algorithm suffers from the weakness in predicting large outlier values.

In Hamilton, the annual average of the deweathered SO_2 mixing ratios were highly consistent with those of the original data as indicated by the close to 1.0 slopes. The deweathered and original annual averages of SO_2 mixing ratios decreased by 23-28% during 1996-2019, which were substantially smaller than the 81% decrease of the corresponding provincial grand total SO_2 emissions during the same period. Such a large discrepancy indicates that the reduction in SO_2 emission in Hamilton likely substantially lagged behind the average provincial level. This is indeed the case since SO_2 emissions from registered facilities in Hamilton (Table S2) fluctuated around $8.67\pm1.75*10^3$ tons $year^{-1}$ during 2002-2009 and then increased to $1.14\pm0.13*10^4$ tons $year^{-1}$ during 2010-2018. This also caused the weak correlations between annual average SO_2 mixing ratio in this city and provincial total SO_2 emission (R^2 = 0.42-0.57, $P<0.05$). In addition, the original annual average SO_2 mixing ratio increased from 3.2-3.5 ppb in 2016-2017 to 4.8-5.0 ppb in 2018-2019 when provincial total SO_2 emission changed little. Thus, reducing local SO_2 emissions in Hamilton is critical to further lower SO_2 mixing ratio in this city in order to meet the CAAQS and the WHO 2021 guideline, despite the existence of other factors such as regional transport (Zhou et al., 2017; Ren et al., 2020).

3.3 Trends in deweathered and original O_3 and O_x mixing ratios

The original annual averages of O_3 and O_x are shown in Fig. S5 and the analysis results of deweathered and original annual averages are listed in Table S5. Increasing trends in

462 the deweathered and original annual average O_3 mixing ratio were obtained in nine
463 cities during the last 2-3 decades, with Halifax as an only exception that showed no
464 significant trend ($P>0.05$) during 2000-2017. Theoretically, the increasing trends in the
465 O_3 mixing ratios could be caused by the enhanced tropospheric photochemical
466 formation of O_3 and/or the weakened titration reaction between O_3 and NO due to the
467 substantial reduction of NO emissions (Simon et al., 2015; Zhou et al., 2017; Sicard et
468 al., 2020; Mitchell et al., 2021; Wang et al., 2022b) (more discussion in Section 4.2
469 below). In contrast, the decreasing trends in the deweathered and original annual
470 average O_x mixing ratios were generally obtained, except in Victoria where there was
471 no significant trend ($P>0.05$) during 2000-2017. The opposite long-term trends between
472 O_3 and O_x suggested that the increase in O_3 is much less than the decrease in NO_2,
473 which does not support the hypothesis of the enhanced tropospheric formation of O_3.
474
475 The deweathered and original annual average O_3 mixing ratios increased by 10 ppb in
476 Edmonton from 1981-2019, 8 ppb in Hamilton from 1996-2019 and Calgary from
477 1986-2014, and <7 ppb in the other cities (Fig. S5, Table S5). The increased O_3 mixing
478 ratio was likely caused by the reduced titration reaction between O_3 and NO,
479 considering the reduced photochemical formation of O_3 in the troposphere (Simon et
480 al., 2015; Xing et al., 2015). Varying weather conditions likely exerted a negligible
481 influence on the decade increases in O_3 mixing ratio in Edmonton, Hamilton, Calgary
482 and Vancouver on the basis of the almost identical increases in deweathered and original
483 annual averages. However, the comparison between deweathered and original annual
484 averages also showed that varying weather conditions did cause an increase of 2 ppb
485 out of the total of 7 ppb increase in the original annual average O_3 in Winnipeg from
486 1985-2018, and 1 ppb increase in Montreal from 1997-2010 and in Toronto from 2003-
487 2019. In contrast, varying weather conditions likely caused 1 ppb decrease in Quebec
488 City from 1995-2019 and in Victoria from 1999-2019.
489
490 The deweathered and original annual average O_x mixing ratio decreased by 10-12 ppb

in Vancouver from 1986-2019, 10 ppb in Halifax from 2000-2019 and in Toronto from 2003-2019, 8-10 ppb in Edmonton from 1981-2019 and <6 ppb in the other cities (Fig. S5 and Table S5). Based on the simultaneously monitored NO mixing ratios and the method reportedly used for estimating the primary NO_2 emission (Kurtenbach et al., 2012; Simon et al., 2015; Casquero-Vera et al., 2019; Xu et al., 2019), the reduced primary NO_2 emissions likely accounted for only 1-2 ppb decrease in O_x in the ten cities and generally acted a minor contributor to the decrease in O_x.

3.4 Trends in deweathered and original $PM_{2.5}$ mass concentrations

Opposite decadal trends were observed between eastern and western Canadian cities in the deweathered and original $PM_{2.5}$ mass concentrations (Table 2, Fig. 3c, 3d and Fig S6). In eastern Canadian cities, either decreasing or no significant trends were obtained in the last two decades. The decreasing trends ($P<0.05$) were identified in the RF-deweathered, BRTs-deweathered and original annual average $PM_{2.5}$ in Montreal from 2005-2019 and in Hamilton from 1998-2019. The overall decreases were only 2 $\mu g\ m^{-3}$ with the decreasing rate of 0.22-0.25 $\mu g\ m^{-3}\ year^{-1}$ in Montreal and 3-4 $\mu g\ m^{-3}$ and 0.14-0.15 $\mu g\ m^{-3}\ year^{-1}$ in Hamilton. The decreasing trends ($P<0.05$) were also identified in the RF-deweathered and BRTs-deweathered $PM_{2.5}$ in Toronto from 2000-2019 with an overall decrease of only 2 $\mu g\ m^{-3}$ and a decreasing rate of only 0.10-0.11 $\mu g\ m^{-3}\ year^{-1}$. However, no significant trend ($P>0.05$) was identified in the original annual average $PM_{2.5}$ in Toronto, implying that the perturbation due to varying weather conditions likely cancelled out the mitigation effects of air pollutants. Note that there were no decreasing trends in the provincial total primary $PM_{2.5}$ emissions in Quebec and Ontario during the periods when $PM_{2.5}$ mass concentration decreased in the above-mentioned three cities. This was not surprising because the major chemical components in $PM_{2.5}$ were derived mainly from secondary sources (Dabek-Zlotorzynska et al., 2019; Jeong et al., 2020; Wang et al., 2021). The decreasing provincial emissions of SO_2, NO_x and volatile organic emissions in Quebec and Ontario likely have reduced the amounts of their oxidized products in $PM_{2.5}$ (Xing et al., 2015; Yao and Zhang, 2019, 2020; Feng

et al., 2020; Jeong et al., 2020; ECCC, 2021; Wang et al., 2021, 2022a). No significant trends ($P>0.05$) were identified in the deweathered and original $PM_{2.5}$ concentrations in Halifax from 2008-2018 and in Quebec City from 1998-2019, which need further investigation.

In western Canadian cities, either increasing or no significant trends were extracted in the deweathered and original annual average $PM_{2.5}$ mass concentrations. Increasing trends ($P<0.05$) were identified in the RF-deweathered, BRTs-deweathered and original annual average $PM_{2.5}$ in Winnipeg from 2001-2018 with an overall increase of only 1-2 $\mu g\ m^{-3}$ and an increasing rate of 0.09-0.10 $\mu g\ m^{-3}\ year^{-1}$. Increasing trends ($P<0.05$) were identified in the RF-deweathered and original annual average $PM_{2.5}$ in Victoria from 1999-2019 with an overall increase of only 1 $\mu g\ m^{-3}$ and an increasing rate of 0.07-0.08 $\mu g\ m^{-3}\ year^{-1}$, but no significant trend was identified in the BRTs-deweathered annual average $PM_{2.5}$. An increasing trend was obtained only in the RF-deweathered annual average $PM_{2.5}$ in Vancouver from 2004-2019, and no significant trends were identified in the BRTs-deweathered and original annual average $PM_{2.5}$. The inconsistency between the trends extracted from the three different annual average $PM_{2.5}$ data series was mostly because of the small magnitudes of the actual interannual changes and thus the trends, which are on the same order of magnitude as the methodology uncertainties. Considering the decreasing trends in NO_2, CO and SO_2 mixing ratios discussed above and the reported decreasing trends in secondary chemical components of $PM_{2.5}$ in Western Canada (Wang et al., 2021, 2022a), the increasing trends in the deweathered and/or original annual average $PM_{2.5}$ observed in some western Canadian cities were likely caused by increased natural emissions, such as from the increased large-scale wildfires in recent years.

It is noticed that a few spikes always appeared in the BRTs-deweathered $PM_{2.5}$ concentrations in the five western Canadian Cities since 2010 (Fig. S6). Most of these spikes were associated with large-scale wildfire emissions (Littell et al., 2009; Collier

et al., 2016; Landis et al., 2018; Matz et al., 2020). For example, wildfires caused large and rapid increases in $PM_{2.5}$ mass concentration from ≤10 μg m^{-3} to >400 μg m^{-3} in Edmonton during 10-12 August 1998 and on 30 May 2019 (Fig. S1). During these periods, the BRTs method predicts the spikes of $PM_{2.5}$. However, the RF method seemingly failed to learn the wildfire signals and missed predicting the spikes associated with largely increased natural emissions because of its inherent weakness.

To further explore the causes for the different trends in $PM_{2.5}$ between eastern and western Canadian cities, the 95^{th}-100^{th} percentile $PM_{2.5}$ mass concentration data in each year were averaged into annual value and were examined below. The top 5% $PM_{2.5}$ exhibited decreasing trends ($P<0.05$) in four eastern Canadian cities and no significant trend ($P>0.05$) in Halifax (Fig. S7). The decreasing trends further confirmed the mitigation effects of air pollutants on $PM_{2.5}$. However, annual average $PM_{2.5}$ was still as high as 8.8 μg m^{-3} in Hamilton in 2019, 7.0-7.7 μg m^{-3} in Quebec City, Toronto and Montreal, and 5.6 μg m^{-3} in Halifax. If keeping the same decreasing rates as mentioned above, it would take another 1-3 decades to lower annual average $PM_{2.5}$ by 2-4 μg m^{-3} in order to meet the WHO 2021 guideline.

No significant trends ($P>0.05$) were identified in the 95^{th}-100^{th} percentile $PM_{2.5}$ mass concentrations in the five western Canadian cities. Note that a large standard deviation of the 95^{th}-100^{th} percentile $PM_{2.5}$ mass concentration was found in some years in the five western cities, indicating a high variability. However, this is not the case in the eastern Canadian cities. The episodic $PM_{2.5}$ events likely canceled out the mitigation effects in the western Canadian cities. The annual average $PM_{2.5}$ were 6.6-6.8 μg m^{-3} in 2019 in Winnipeg, Edmonton and Victoria, which need great additional mitigation efforts in order to reduce to a level below 5 μg m^{-3} in the presence of the episodes caused by natural emissions. Note that the annual average $PM_{2.5}$ was already lower than 5 μg m^{-3} in Vancouver, and that the annual average was 8.4 μg m^{-3} at the study site in Calgary in 2014. The value slightly decreased to 7.6 μg m^{-3} in 2019 at another site ~5 km from

the study site in Calgary.

3.5 Trends in AQHI in the ten Canadian cities

Decreasing trends in AQHI were obtained in nine cities ($P<0.05$), with Calgary as an only exception (Figs. S9 and S10). The annual average AQHI decreased by 8-29% during the last two decades to the levels of 1.8 to 3.0 during 2017-2019 in the nine cities. In Calgary, the annual averages AQHI narrowed around 3.4±0.2 during 1998-2010. In the five eastern cities, AQHI above 10 occurred at <0.3% frequency before 2010, but none after 2010. AQHI between 7-10 occurred at <4% frequency before 2010, and below 0.5% after 2010. In the five western cities, AQHI above 10 occurred at <0.3% frequency, and AQHI between 7-10 occurred at <2% frequency during the last two decades. Note that AQHI above 10 still occurred at <0.3% frequency even after 2010 because of the large-scale wildfires. In fact, the occurrence frequencies of AQHI between 7-10 and above 10 were a bit higher after 2010 (<0.3%) than before 2010 in Vancouver and Victoria due to the increased wildfire events in the most recent decade.

On seasonal average, AQHI above 10 occurred most in summer (from June to August) in most cities, e.g., Victoria (1.1%), Vancouver (0.8%), Edmonton (0.7%) and Winnipeg (0.1%) in 2018. AQHI above 10 also occurred in winter (from December to February next year) and spring (from March to May) in some cities, e.g., Edmonton (0.3% in the spring of 2019 and 0.1-0.3% in the winter of 2012-2013) and Winnipeg (0.1% in the spring of 2018).

4. Discussion

4.1 Perturbations due to varying weather conditions on the decadal trends

Perturbations due to varying weather conditions on the decadal trends of the studied pollutants are presented in detail in Section 3 above, and key findings are briefly summarized here. The perturbations are defined as the percentage differences between the trends of the original and deweathered annual average concentrations. In ~70% of

the studies cases covering all the selected criteria pollutants in the ten cities, the perturbation due to varying weather conditions had an influence of within ±2% on the decadal trends of the original annual averages over the 20-year period. In the remaining cases, relatively larger perturbations were identified, but at most 16%, keeping in mind that a portion of the percentage differences between the trends of the original and deweathered annual average concentrations was likely caused by errors inherent from BRTs and RF predictions.

Specifically, in all the cases except CO in Quebec City (for which the calculated perturbation is 7% from BRTs and 12% from RF), at least one of the two machining leaning methods generated a perturbation of smaller than 5%. For example, the top three largest perturbations obtained from using one of the two machining leaning methods were all for SO_2, including 16% from RF in Winnipeg, 14% from BRTs in Montreal and 13% from RF from BRTs in Toronto; however, the corresponding perturbations from using another one of the two machining leaning methods were quite smaller (4%, 0.2% and 3%, respectively), indicating possible large methodology uncertainties. Thus, perturbations due to varying weather conditions should be generally small on the two-decade time scale in most cases.

4.2 Trend analysis of O_3 net sinks and sources

As reported in literature, a large fraction of ground-level O_3 at middle-high latitude zones comes from secondary reactions associated with natural sources (Barrie et al., 1988; Van Dam et al., 2013; Cooper et al., 2005; Seinfeld and Pandis, 2006; Mitchell et al., 2021). The natural signal usually has a spring maximum related to stratosphere-troposphere exchange as well as increasing photochemistry, among other potential factors (Chan and Vet, 2010; Monks et al., 2015; Strode et al., 2018; Xu et al., 2019). The contributions from stratosphere-troposphere exchange are approximately 40 ppb, while the sinks associated with natural and anthropogenic factors in the atmospheric boundary layer may decrease the ground-level O_3 to levels lower than 40 ppb (Barrie

et al., 1988; Van Dam et al., 2013; Chan and Vet, 2010; Monks et al., 2015; Mitchell et al., 2021). On the other hand, enhanced tropospheric photochemical reactions under favorable meteorological conditions may increase the ground-level O_3 to levels higher than 40 ppb, causing severe O_3 pollution (Monks et al., 2015; Simon et al., 2015; Seinfeld and Pandis 2006; Xu et al., 2019). In fact, 40 ppb has been widely used as the threshold value for assessing O_3 impacts on ecosystem health (e.g., AOT40 index) (Avnery et al., 2011). Thus, O_3 data with mixing ratios lower and higher than 40 ppb were analyzed separately below, with the former case representing net O_3 sinks occurring in the atmospheric boundary layer and the latter one representing net O_3 sources occurring therein (Table 3).

In the cases with O_3 mixing ratios ≥ 40 ppb, the deweathered and original values, however, exhibited decreasing trends ($P<0.05$) in all of the five eastern cities and two western cities (Victoria and Vancouver) (Figs. 4 and S8 and Table 3). The overall decreases in O_3 with mixing ratios ≥ 40 ppb were 2 ppb in Halifax from 2000-2017, in Montreal and Quebec City from 1995-2019, and in Victoria from 1999-2019 (figure not provided), 4 ppb in Toronto from 2003-2019, 5-6 ppb in Hamilton from 1987-2019, and 12 ppb in Vancouver from 1986-2019 (but only 2 ppb from 2000-2019). Again, a few spikes and troughs occurred in the BRTs-deweathered values possibly because of unpredictably increased and decreased emissions of O_3 precursors, respectively. In the cases with O_x mixing ratios ≥ 40 ppb, the decreasing trends were obtained in all of the ten cities. These results further implied that the tropospheric photochemical formation of O_3 likely reduced in seven of the ten cities during the last two to three decades.

In the cases with O_3 mixing ratios ≥ 40 ppb in the remaining three western cities, the decreasing trends ($P<0.05$) were obtained in the BRTs-deweathered and original values and no significant trend ($P>0.05$) in the RF-deweathered values in Winnipeg; the decreasing trend was obtained only in the original values in Calgary; and no significant trends in the deweathered and original values in Edmonton. These trend results implied

665 that the responses of the fraction of O_3 to emission reductions of its precursors were too
666 weak to be confirmed, especially in the presence of perturbation due to varying weather
667 conditions.
668
669 In the cases with O_3 mixing ratios < 40 ppb, the trends were almost the same as those
670 from using the full dataset of O_3 mixing ratios. This consistency suggested that the
671 increasing trends in O_3 mixing ratio in the nine Canadian cities were mainly due to the
672 reduced O_3 sinks.
673
674 *4.3 The perturbation from large-scale wildfires on $PM_{2.5}$ trend in western Canadian*
675 *cities*
676 Wildfire emissions become important contributors to air pollution in North America
677 with global warning and increased extreme weather conditions such as heatwaves and
678 severe droughts (Andreae and Merlet, 2001; Littell et al., 2009; Marlon et al., 2013;
679 Barbero et al., 2015; Abatzoglou and Williams, 2016; Randerson et al., 2017; Mardi et
680 al., 2021). For example, Meng et al. (2019) estimated that wildfires accounted for 17.1%
681 of the total population-weighted exposure to $PM_{2.5}$ for Canadians during 2013-2015
682 and 2017-2018. The large contribution was not surprising because large wildfires can
683 rapidly increase hourly $PM_{2.5}$ mass concentration from a few $\mu g\ m^{-3}$ to >400 $\mu g\ m^{-3}$
684 (Landis et al., 2018 and Fig. S1). The estimated annual economic cost attributable to
685 $PM_{2.5}$ pollution reached $410M-$1.8B for acute health impacts and $4.3B-$19B for
686 chronic health impacts in western Canada (Landis et al., 2018; Matz et al., 2020). In the
687 U.S., wildfire emissions were reported to account for up to 25% of annual primary
688 $PM_{2.5}$ emissions (U.S. EPA, 2014).
689
690 Due to the wide occurrence of small-scale wildfires, most of the emitted air pollutants
691 from these sources and subsequent long-range transport can be considered as natural
692 background pollution. The key issue is to quantify the abnormally increased
693 contributions from large-scale wildfires to annual average $PM_{2.5}$ in each year and their

perturbations on long-term trends in $PM_{2.5}$. Using the method described in Section 2, the perturbation contributions in Winnipeg were estimated to be around 0.5±0.4 μg m^{-3} in 2001-2018, with larger values of 1.1-1.3 μg m^{-3} associated with large-scale wildfires in 2002, 2012 and 2018 (Fig. 5a). The larger perturbation contributions in 2012 and 2018 indeed led to an increasing trend in $PM_{2.5}$ from 2001-2018 in this city (Table 2). The perturbation contributions were, however, smaller than 0.2 μg m^{-3} in 2001, 2003, 2005, 2006, 2008, 2009, 2014 and 2017, and such small values may be related to varying weather conditions rather than large-scale wildfires.

In Edmonton, the perturbation contributions were around 1.0±0.9 μg m^{-3} in 1998-2019 (Fig. 5b). However, the largest contribution was 3.0 μg m^{-3} in 1998, followed by 2.4 μg m^{-3} in 2018 and 2.1 μg m^{-3} in 2004, respectively, because of large-scale wildfires. The perturbation contributions from large-scale wildfires were large enough to cancel out the mitigation effect of air pollutants on annual averages of $PM_{2.5}$ in Edmonton. In Calgary, the perturbation contributions were around 1.2±0.7 μg m^{-3} in 1998-2013, depending on if large-scale wildfires occurred in any particular year. For example, the perturbation contributions were smaller than 0.2 μg m^{-3} in 1999, 2007 and 2013, while the contributions reached 2.2-2.3 μg m^{-3} in 1998 and 2010.

In Victoria, the perturbation contributions were around 0.7±0.2 μg m^{-3} in 1998-2019., The perturbation contribution in each year was, however, larger than 0.4 μg m^{-3}, suggesting that the wildfires were always important contributors. In Vancouver, the perturbation contributions largely decreased to 0.3±0.5 μg m^{-3} in 2004-2019. However, the maximum value still reached 1.7 μg m^{-3} in 2017, followed by 1.4 μg m^{-3} in 2018 and 0.5 μg m^{-3} in 2015. The large perturbation likely overwhelmed or canceled out the effects of emission reductions on annual average $PM_{2.5}$.

5. Conclusions

Through analysis of deweathered and original annual average concentrations of selected criteria air pollutants measured in ten major cities in Canada during the last 2-3 decades, we have generated the following decadal trends for these pollutants: 1) decreasing trends in NO_2, CO and SO_2 mainly due to reduced primary emissions across Canada, except no significant trend in CO in Montreal; 2) increasing trends in O_3 mainly due to the reduced titration effect across Canada, except no significant trend in O_3 in Halifax; and 3) roughly opposite trends in $PM_{2.5}$ between eastern and western Canada, resulted from the combined effects of emission reductions and the occurrence of large-scale wildfires.

The overall percentage decrease in NO_2 during the last 2-3 decades among the 10 cities ranged from 37% to 62%, and the annual decreasing rates varied from 0.31 ppb year $^{-1}$ to 0.74 ppb year $^{-1}$. The overall percentage decrease in CO varied from 57% to 92% and the annual decreasing rate ranged from 0.010 ppm year^{-1} to 0.076 ppm year^{-1} between nine cities. The corresponding numbers for SO_2 are from 23% to 93% and from 0.04 ppb year^{-1} to 0.63 ppb year^{-1} among the 10 cities. By only considering O_3 mixing ratio $\geq$ 40 ppb, annual average O_3 decreased by 2-4 ppb in most cities during the past two-three decades, but not in Calgary and Edmonton, and no consistent decreasing trend was identified in Winnipeg, implying that the mitigation effects of air pollutants on O_3 were too weak to be confirmed.

The mitigation effects on $PM_{2.5}$ were detected on the basis of the identified decreasing trends in three of the five eastern cities regardless of using original or deweathered annual average data, but this is not the case in the other two eastern cities. In the five western cities, the perturbation due to large-scale wildfires greatly affected original annual average $PM_{2.5}$ and was large enough to cancel out the mitigation effects in some years, leading to no decreasing trends and in some cases even increasing trends.

Excluding Calgary, the annual average AQHI showed a significant decrease by 8-29% during the last two decades to levels between 1.8 and 3.0 in 2017-2019. However, large-scale wildfire events still occasionally elevated AQHI to a level of above 10 (very high risk) (<0.3% frequency) in western Canadian cities after 2010. Thus, large-scale wildfires have become a key factor in causing severe air pollution in Canadian cities, as was seen in the most recent very large-scale wildfires occurred in Canada from the later spring to the earlier summer in 2023 that resulted in severe air pollution across Canada and New York through long-range transport. Urgent work should be conducted for assessing the impacts of large-scale wildfires on human health and climate change, besides investigating their occurrence and control mechanisms and transport pathways. In-depth studies are also needed to explore the causes of the non-decreasing trends in O_3 with mixing ratios ≥ 40 ppb in some western Canadian cities, results from which are critical for making future control policies.

Acknowledgement. We greatly appreciate all the personnel of the NAPS Partners who operate the sites across Canada and collect the field samples, and the staff of the Analysis and Air Quality section in Ottawa for the laboratory chemical analyses and QA/QC of the data used in the present study. NPRI/APEI groups are also acknowledged for their efforts in generating emissions data across Canada.

Data availability. the data used in this paper are downloadable from https://open.canada.ca/data/en/dataset/1b36a356-defd-4813-acea-47bc3abd859b) and https://www.canada.ca/en/environment-climate-change/services/environmental-indicators/air-pollutant-emissions.html.

Author contributions. XY and LZ designed the research, conducted analysis, and prepared the manuscript.

Competing interests. One of the coauthors is a member of the editorial board of ACP.

References

781 Abatzoglou, J. T. and Williams, A. P.: Impact of anthropogenic climate change on
782 wildfire across western US forests, Proc. Natl. Acad. Sci. USA., 113, 11770-11775,
783 https://doi.org/10.1073/pnas.1607171113, 2016.
784 Al-Abadleh, H. A., Lysy, M., Neil, L., Patel, P., Mohammed, W., and Khalaf, Y.:
785 Rigorous quantification of statistical significance of the COVID-19 lockdown effect
786 on air quality: The case from ground-based measurements in Ontario, Canada, J.
787 Hazard. Mater., 413, 125445, https://doi.org/10.1016/j.jhazmat.2021.125445, 2021.
788 Andreae, M. O. and Merlet, P.: Emission of trace gases and aerosols from biomass
789 burning, Global. Biogeochem. Cy., 15, 955-966,
790 https://doi.org/10.1029/2000GB001382, 2001.
791 Astitha, M., Luo, H., Rao, S. T., Hogrefe, C., Mathur, R., and Kumar, N.: Dynamic
792 Evaluation of Two Decades of WRF-CMAQ Ozone Simulations over the
793 Contiguous United States, Atmos. Environ., 164, 102-116,
794 https://doi.org/10.1016/j.atmosenv.2017.05.020, 2017.
795 Avnery, S., Mauzerall, D.L., Liu, J., Horowitz, L.W.: Global crop yield reductions due
796 to surface ozone exposure: 2. Year 2030 potential crop production losses and
797 economic damage under two scenarios of O3 pollution. Atmos. Environ., 45, 2297-
798 2309, https://doi.org/10.1016/j.atmosenv.2010.11.045, 2011.
799 Aziz, J. J., Ling, M., Rifai, H. S., Newell, C. J., and Gonzales, J. R.: MAROS: a decision
800 support system for optimizing monitoring plans, Ground. Water., 41, 355-367,
801 https://doi.org/10.1111/j.1745-6584.2003.tb02605.x, 2003.
802 Barbero, R., Abatzoglou, J. T., Larkin, N. K., Kolden, C. A., and Stocks, B.: Climate
803 change presents increased potential for very large fires in the contiguous United
804 States, Int. J. Wildland. Fire., 24, https://doi.org/10.1071/WF15083, 2015.
805 Bari, M.A., Kindzierski, W.B. Eight-year (2007–2014) trends in ambient fine
806 particulate matter ($PM_{2.5}$) and its chemical components in the Capital Region of
807 Alberta, Canada. Environment Int. 91, 122–132,
808 http://doi:10.1016/j.envint.2016.02.033, 2016.
809 Barrie, L. A., Bottenheim, J. W., Schnell, R. C., Crutzen, P. J., and Rasmussen, R. A.:
810 Ozone destruction and photochemical reactions at polar sunrise in the lower Arctic
811 atmosphere, Nature, 334, 138-141, https://doi.org/10.1038/334138A0, 1988.
812 Bowdalo, D., Petetin, H., Jorba, O., Guevara, M., Soret, A., Bojovic, D., Terrado, M.,
813 Querol, X., and Pérez García-Pando, C.: Compliance with 2021 WHO air quality

814 guidelines across Europe will require radical measures, Environ. Res. Lett., 17,
815 https://doi.org/10.1088/1748-9326/ac44c7, 2022.
816 Carslaw, D. C. and Taylor, P. J.: Analysis of air pollution data at a mixed source location
817 using boosted regression trees, Atmos. Environ., 43, 3563-3570,
818 https://doi.org/10.1016/j.atmosenv.2009.04.001, 2009.
819 Carslaw, D. C. and Ropkins, K.: openair — An R package for air quality data analysis,
820 Environ. Modell. Softw., 27-28, 52-61,
821 https://doi.org/10.1016/j.envsoft.2011.09.008, 2012.
822 Carslaw, D. C.: Worldmet: Import Surface Meteorological Data from NOAA Integrated
823 Surface Database (ISD), R package version 0.9.5, https://cran.r-
824 project.org/package=worldmet. 2021.
825 Casquero-Vera, J. A., Lyamani, H., Titos, G., Borras, E., Olmo, F. J., and Alados-
826 Arboledas, L.: Impact of primary NO_2 emissions at different urban sites exceeding
827 the European NO_2 standard limit, Sci. Total. Environ., 646, 1117-1125,
828 https://doi.org/10.1016/j.scitotenv.2018.07.360, 2019.
829 Chan, E. and Vet, R. J.: Baseline levels and trends of ground level ozone in Canada and
830 the United States, Atmos. Chem. Phys., 10, 8629-8647, https://doi.org/10.5194/acp-
831 10-8629-2010, 2010.
832 Collier, S., Zhou, S., Onasch, T. B., Jaffe, D. A., Kleinman, L., Sedlacek, A. J., 3rd,
833 Briggs, N. L., Hee, J., Fortner, E., Shilling, J. E., Worsnop, D., Yokelson, R. J.,
834 Parworth, C., Ge, X., Xu, J., Butterfield, Z., Chand, D., Dubey, M. K., Pekour, M.
835 S., Springston, S., and Zhang, Q.: Regional Influence of Aerosol Emissions from
836 Wildfires Driven by Combustion Efficiency: Insights from the BBOP Campaign,
837 Environ. Sci. Technol., 50, 8613-8622, https://doi.org/10.1021/acs.est.6b01617,
838 2016.
839 Cooper, O. R.: A springtime comparison of tropospheric ozone and transport pathways
840 on the east and west coasts of the United States, J. Geophys. Res., 110,
841 https://doi.org/10.1029/2004JD005183, 2005.
842 Dabek-Zlotorzynska, E., Celo, V., Ding, L., Herod, D., Jeong, C.-H., Evans, G., and
843 Hilker, N.: Characteristics and sources of $PM_{2.5}$ and reactive gases near roadways
844 in two metropolitan areas in Canada, Atmos. Environ., 218,
845 https://doi.org/10.1016/j.atmosenv.2019.116980, 2019.
846 Dabek-Zlotorzynska, E., Dann, T. F., Kalyani Martinelango, P., Celo, V., Brook, J. R.,

Mathieu, D., Ding, L., and Austin, C. C.: Canadian National Air Pollution Surveillance (NAPS) $PM_{2.5}$ speciation program: Methodology and $PM_{2.5}$ chemical composition for the years 2003–2008, Atmos. Environ., 45, 673-686, https://doi.org/10.1016/j.atmosenv.2010.10.024, 2011.

Dai, Q., Hou, L., Liu, B., Zhang, Y., Song, C., Shi, Z., Hopke, P. K., and Feng, Y.: Spring Festival and COVID-19 Lockdown: Disentangling PM Sources in Major Chinese Cities, Geophys. Res. Lett., 48, e2021GL093403, https://doi.org/10.1029/2021gl093403, 2021.

ECCC, Environment and Climate Change Canada: Canadian Environmental Sustainability Indicators: Air pollutant emissions, available at: https://www.canada.ca/en/environment-climate-change/services/environmental-indicators/air-pollutant-emissions.html, last access: 20 October 2023.

ECCC, Environment and Climate Change Canada: (2023) Canadian Environmental Sustainability Indicators: Air Quality. Available at: www.canada.ca/en/environment-climate-change/services/environmental-indicators/air-quality.html., last access 20 October 2023.

Feng, J., Chan, E., Vet, R. Air quality in the eastern United States and Eastern Canada for 1990–2015: 25 years of change in response to emission reductions of SO_2 and NO_x in the region. Atmos. Chem. Phys., 20, 3107–3134, https://doi.org/10.5194/acp-20-3107-2020

Foley, K. M., Hogrefe, C., Pouliot, G., Possiel, N., Roselle, S. J., Simon, H., and Timin, B.: Dynamic evaluation of CMAQ part I: Separating the effects of changing emissions and changing meteorology on ozone levels between 2002 and 2005 in the eastern US, Atmos. Environ., 103, 247-255, https://doi.org/10.1016/j.atmosenv.2014.12.038, 2015.

Grange, S. K. and Carslaw, D. C.: Using meteorological normalisation to detect interventions in air quality time series, Sci. Total. Environ., 653, 578-588, https://doi.org/10.1016/j.scitotenv.2018.10.344, 2019.

Grange, S. K., Carslaw, D. C., Lewis, A. C., Boleti, E., and Hueglin, C.: Random forest meteorological normalisation models for Swiss PM_{10} trend analysis, Atmos. Chem. Phys., 18, 6223-6239, https://doi.org/10.5194/acp-18-6223-2018, 2018.

Griffin, D., McLinden, C. A., Racine, J., Moran, M. D., Fioletov, V., Pavlovic, R., Mashayekhi, R., Zhao, X., and Eskes, H.: Assessing the Impact of Corona-Virus-19

on Nitrogen Dioxide Levels over Southern Ontario, Canada, Remote Sens-Basel, 12, https://doi.org/10.3390/rs12244112, 2020.

Health Canada. 2021. Health impacts of air pollution in Canada – Estimate of morbidity and premature mortality outcomes – 2021 report. Government of Canada. ISBN 978-0-660-37331-7. 56 pp. https://www.canada.ca/content/dam/hc-sc/documents/services/publications/healthy-living/2021-health-effects-indoor-air-pollution/hia-report-eng.pdf

Jeong, C.-H., Traub, A., Huang, A., Hilker, N., Wang, J. M., Herod, D., Dabek-Zlotorzynska, E., Celo, V., and Evans, G. J.: Long-term analysis of $PM_{2.5}$ from 2004 to 2017 in Toronto: Composition, sources, and oxidative potential, Environ. Pollut., 263, https://doi.org/10.1016/j.envpol.2020.114652, 2020.

Kampata, J. M., Parida, B. P., and Moalafhi, D. B.: Trend analysis of rainfall in the headstreams of the Zambezi River Basin in Zambia, Phys. Chem. Earth., 33, 621-625, https://doi.org/10.1016/j.pce.2008.06.012, 2008.

Kurtenbach, R., Kleffmann, J., Niedojadlo, A., and Wiesen, P.: Primary NO_2 emissions and their impact on air quality in traffic environments in Germany, Environ. Sci. Eur., 24, https://doi.org/10.1186/2190-4715-24-21, 2012.

https://doi.org/10.1016/j.envpol.2020.115900, 2021.

Landis, M. S., Edgerton, E. S., White, E. M., Wentworth, G. R., Sullivan, A. P., and Dillner, A. M.: The impact of the 2016 Fort McMurray Horse River Wildfire on ambient air pollution levels in the Athabasca Oil Sands Region, Alberta, Canada, Sci. Total. Environ., 618, 1665-1676, https://doi.org/10.1016/j.scitotenv.2017.10.008, 2018.

Lin, Y., Zhang, L., Fan, Q., Meng, H., Gao, Y., Gao, H., and Yao, X.: Decoupling impacts of weather conditions on interannual variations in concentrations of criteria air pollutants in south China–constraining analysis uncertainties by using multiple analysis tools, Atmos. Chem. Phys., 22, 16073–16090, https://doi.org/10.5194/acp-22-16073-2022, 2022

Littell, J. S., McKenzie, D., Peterson, D. L., and Westerling, A. L.: Climate and wildfire area burned in western U.S. ecoprovinces, 1916-2003, Ecol. Appl., 19, 1003-1021, https://doi.org/10.1890/07-1183.1, 2009.

Lovric, M., Pavlovic, K., Vukovic, M., Grange, S. K., Haberl, M., and Kern, R.: Understanding the true effects of the COVID-19 lockdown on air pollution by

means of machine learning, Environ. Pollut., 274, 115900.

Ma, R., Ban, J., Wang, Q., Zhang, Y., Yang, Y., He, M. Z., Li, S., Shi, W., and Li, T.: Random forest model based fine scale spatiotemporal O_3 trends in the Beijing-Tianjin-Hebei region in China, 2010 to 2017, Environ. Pollut., 276, 116635, https://doi.org/10.1016/j.envpol.2021.116635, 2021.

Mallet, M. D.: Meteorological normalisation of PM_{10} using machine learning reveals distinct increases of nearby source emissions in the Australian mining town of Moranbah, Atmos. Pollut. Res., 12, 23-35, https://doi.org/10.1016/j.apr.2020.08.001, 2021.

Mardi, A. H., Dadashazar, H., Painemal, D., Shingler, T., Seaman, S. T., Fenn, M. A., Hostetler, C. A., and Sorooshian, A.: Biomass Burning Over the United States East Coast and Western North Atlantic Ocean: Implications for Clouds and Air Quality, J. Geophys. Res.-Atmos., 126, https://doi.org/doi:10.1029/2021JD034916, 2021.

Marlon, J. R., Bartlein, P. J., Daniau, A.-L., Harrison, S. P., Maezumi, S. Y., Power, M. J., Tinner, W., and Vanniére, B.: Global biomass burning: a synthesis and review of Holocene paleofire records and their controls, Quaternary. Sci. Rev., 65, 5-25, https://doi.org/10.1016/j.quascirev.2012.11.029, 2013.

Matz, C. J., Egyed, M., Xi, G., Racine, J., Pavlovic, R., Rittmaster, R., Henderson, S. B., and Stieb, D. M.: Health impact analysis of $PM_{2.5}$ from wildfire smoke in Canada (2013-2015, 2017-2018), Sci. Total. Environ., 725, 138506, https://doi.org/10.1016/j.scitotenv.2020.138506, 2020.

Meng, J., Martin, R. V., Li, C., van Donkelaar, A., Tzompa-Sosa, Z. A., Yue, X., Xu, J. W., Weagle, C. L., and Burnett, R. T.: Source Contributions to Ambient Fine Particulate Matter for Canada, Environ. Sci. Technol., 53, 10269-10278, https://doi.org/10.1021/acs.est.9b02461, 2019.

Mitchell, M., Wiacek, A., and Ashpole, I.: Surface ozone in the North American pollution outflow region of Nova Scotia: Long-term analysis of surface concentrations, precursor emissions and long-range transport influence, Atmos. Environ., 261, https://doi.org/10.1016/j.atmosenv.2021.118536, 2021.

Monks, P. S., Archibald, A. T., Colette, A., Cooper, O., Coyle, M., Derwent, R., Fowler, D., Granier, C., Law, K. S., Mills, G. E., Stevenson, D. S., Tarasova, O., Thouret, V., von Schneidemesser, E., Sommariva, R., Wild, O., and Williams, M. L.: Tropospheric ozone and its precursors from the urban to the global scale from air

quality to short-lived climate forcer, Atmos. Chem. Phys., 15, 8889-8973, https://doi.org/10.5194/acp-15-8889-2015, 2015.

Munir, S., Luo, Z., and Dixon, T.: Comparing different approaches for assessing the impact of COVID-19 lockdown on urban air quality in Reading, UK, Atmos. Res., 261, 105730, https://doi.org/10.1016/j.atmosres.2021.105730, 2021.

Pappin, A. J., Hakami, A., Blagden, P., Nasari, M., Szyszkowicz, M., and Burnett, R. T.: Health benefits of reducing NOx emissions in the presence of epidemiological and atmospheric nonlinearities, Environ. Res. Lett., 11, https://doi.org/10.1088/1748-9326/11/6/064015, 2016.

Randerson, J.T., G.R. van der Werf, L. Giglio, G.J. Collatz, and P.S. Kasibhatla. 2017. Global Fire Emissions Database, Version 4.1 (GFEDv4). ORNL DAAC, Oak Ridge, Tennessee, USA. https://doi.org/10.3334/ORNLDAAC/1293.

Ren, S., Stroud, C., Belair, S., Leroyer, S., Munoz-Alpizar, R., Moran, M., Zhang, J., Akingunola, A., and Makar, P.: Impact of Urbanization on the Predictions of Urban Meteorology and Air Pollutants over Four Major North American Cities, Atmosphere-Basel, 11, https://doi.org/10.3390/atmos11090969, 2020.

Seinfeld, J.H. and Pandis, S.N. (2006) Atmospheric Chemistry and Physics: From Air Pollution to Climate Change. 2nd Edition, John Wiley & Sons, New York.

Shi, X. and Brasseur, G. P.: The Response in Air Quality to the Reduction of Chinese Economic Activities During the COVID-19 Outbreak, Geophys. Res. Lett., 47, e2020GL088070, https://doi.org/10.1029/2020GL088070, 2020.

Shi, Z., Song, C., Liu, B., Lu, G., Xu, J., Van Vu, T., Elliott, R. J. R., Li, W., Bloss, W. J., and Harrison, R. M.: Abrupt but smaller than expected changes in surface air quality attributable to COVID-19 lockdowns, Sci. Adv. Mater., 7, https://doi.org/10.1126/sciadv.abd6696, 2021.

Sicard, P., De Marco, A., Agathokleous, E., Feng, Z., Xu, X., Paoletti, E., Rodriguez, J. J. D., and Calatayud, V.: Amplified ozone pollution in cities during the COVID-19 lockdown, Sci. Total. Environ., 735, 139542, https://doi.org/10.1016/j.scitotenv.2020.139542, 2020.

Simon, H., Reff, A., Wells, B., Xing, J., and Frank, N.: Ozone trends across the United States over a period of decreasing NO_x and VOC emissions, Environ. Sci. Technol., 49, 186-195, https://doi.org/10.1021/es504514z, 2015.

Stieb, D.M.; Burnett, R.T.; Smith-Doiron, M.; Brion, O.; Shin, H.H.; Economou, V.: A

new multipollutant, no-threshold air quality health index based on short-term associations observed in daily time-series analyses, J. Air Waste Manag. Assoc. 58, 435–450, https://doi.org/10.3155/1047-3289.58.3.435, 2008.

Strode, S. A., Ziemke, J. R., Oman, L. D., Lamsal, L. N., Olsen, M. A., and Liu, J.: Global changes in the diurnal cycle of surface ozone, Atmos. Environ., 199, 323-333, https://doi:10.1016/j.atmosenv.2018.11.028, 2019.

To T., Shen S., Atenafu E.G., Guan J., McLimont S., Stocks B.: The Air Quality Health Index and asthma morbidity: A population-based study. *Environ Health Perspect.* 121:46–52; https://ehp.niehs.nih.gov/doi/10.1289/ehp.1104816, 2013.

Van Dam, B., Helmig, D., Burkhart, J. F., Obrist, D., and Oltmans, S. J.: Springtime boundary layer O_3 and GEM depletion at Toolik Lake, Alaska, J. Geophys. Res.-Atmos., 118, 3382-3391, https://doi.org/10.1002/jgrd.50213, 2013.

Vu, T. V., Shi, Z., Cheng, J., Zhang, Q., He, K., Wang, S., and Harrison, R. M.: Assessing the impact of clean air action on air quality trends in Beijing using a machine learning technique, Atmos. Chem. Phys., 19, 11303-11314, https://doi.org/10.5194/acp-19-11303-2019, 2019.

Wang, H., Zhang, L., Yao, X., Cheng, I., and Dabek-Zlotorzynska, E.: Identification of decadal trends and associated causes for organic and elemental carbon in $PM_{2.5}$ at Canadian urban sites, Environ. Int., 159, 107031, https://doi.org/10.1016/j.envint.2021.107031, 2022a.

Wang, H.; Lu, X.; Jacob, D.J.; Cooper, O.R.; Chang, K.L.; Li, K.; Gao, M.; Liu, Y.; Sheng, B.; Wu, K.; Wu, T.; Zhang, J.; Sauvage, B.; Nédélec, P.; Blot, R.; Fan, S. Global tropospheric ozone trends, attributions, and radiative impacts in 1995–2017: an integrated analysis using aircraft (IAGOS) observations, ozonesonde, and multi-decadal chemical model simulations. *Atmos. Chem. Phys.*, *22*, 13753-13782, https://doi.org/10.5194/acp-22-13753-2022, 2022b.

Wang, H., Zhang, L., Cheng, I., Yao, X., and Dabek-Zlotorzynska, E.: Spatiotemporal trends of $PM_{2.5}$ and its major chemical components at urban sites in Canada, J. Environ. Sci-China., 103, 1-11, https://doi.org/10.1016/j.jes.2020.09.035, 2021.

Wang, Y., Wen, Y., Wang, Y., Zhang, S., Zhang, K. M., Zheng, H., Xing, J., Wu, Y., and Hao, J.: Four-Month Changes in Air Quality during and after the COVID-19 Lockdown in Six Megacities in China, Environ. Sci. Tech. Let., 7, 802-808, https://doi.org/10.1021/acs.estlett.0c00605, 2020.

WHO, WHO global air quality guidelines: Particulate matter ($PM_{2.5}$ and PM_{10}), ozone, nitrogen dioxide, sulfur dioxide and carbon monoxide, ISBN-13: 978-92-4-003421-1, https://www.who.int/publications/i/item/9789240034228, 2021.

Xing, J., Mathur, R., Pleim, J., Hogrefe, C., Gan, C. M., Wong, D. C., Wei, C., Gilliam, R., and Pouliot, G.: Observations and modeling of air quality trends over 1990–2010 across the Northern Hemisphere: China, the United States and Europe, Atmos. Chem. Phys., 15, 2723-2747, https://doi.org/10.5194/acp-15-2723-2015, 2015.

Xu, X., Zhang, T., and Su, Y.: Temporal variations and trend of ground-level ozone based on long-term measurements in Windsor, Canada, Atmos. Chem. Phys., 19, 7335-7345, https://doi.org/10.5194/acp-19-7335-2019, 2019.

Yao, J., Stieb, D.M., Taylor, E., Henderson, S.: Assessment of the air quality health index (AQHI) and four alternate AQHI-Plus amendments for wildfire seasons in British Columbia. Can J Public Health 111, 96–106. https://doi.org/10.17269/s41997-019-00237-w, 2020.

Yao, X. and Zhang, L.: Causes of large increases in atmospheric ammonia in the last decade across North America. ACS Omega, 11, 4(26), 22133-22142, https:// doi: 10.1021/acsomega.9b03284, 2019.

Yao, X. and Zhang, L.: Decoding long-term trends in the wet deposition of sulfate, nitrate, and ammonium after reducing the perturbation from climate anomalies, Atmos. Chem. Phys., 20, 721-733, https://doi.org/10.5194/acp-20-721-2020, 2020.

Zhang, T., Xu, X., and Su, Y.: Long-term measurements of ground-level ozone in Windsor, Canada and surrounding areas, Chemosphere, 294, 133636, https://doi.org/10.1016/j.chemosphere.2022.133636, 2022.

Zhou, Y., Mao, H., Demerjian, K., Hogrefe, C., and Liu, J.: Regional and Hemispheric Influences on Temporal Variability in Baseline Carbon Monoxide and Ozone over the Northeast US, Atmos. Environ. 164, 309-324, http://dx.doi.org/10.1016/j.atmosenv.2017.06.017, 2017.

Table 1. Regression of (BRTs and RF) deweathered against original annual average NO_2 mixing ratios, annual decreasing rate (ppb $year^{-1}$) and overall decreasing percentage (%) of deweathered and original NO_2 mixing ratios ($P<0.05$ for all the decreasing trends), correlation (R^2) of deweathered and original NO_2 mixing ratios against provincial total NO_x emissions and transportation NO_x emissions ($P<0.05$ except those marked with "/" for which $p>0.05$), and percentage decreases (%) of the provincial total NO_x emissions and transportation NO_x emissions ($P<0.05$ for all the decreasing trends except increasing trends in NO_x emission from 1990-2010 in Winnipeg and Calgary[#]) in ten Canadian cities during the last decades ([##]since 1990; bold font numbers represent cases with smaller deceasing percentages in NO_2 mixing ratios than in corresponding provincial emissions, italic numbers represent $R^2>0.8$, and italic bold numbers represent an increasing trend).

City	Regression of deweathered against original mixing ratio ($P<0.01$)		Annual decreasing rate (ppb $year^{-1}$) and overall decreasing percentage (%) ($P<0.05$)			Correlation (R^2) of mixing ratios against provincial total and transportation NO_x emissions ($P<0.05$)			Percentage decreases (%) of provincial total and transportation emissions[&&]
	BRTs	RF	BRTs	RF	original	BRTs	RF	original	
Halifax (1996-2017)	y=1.03*x	y=1.08*x	0.49, 62	0.45, 58	0.55, 50	*0.83*, *0.84*	*0.84*, *0.85*	*0.86*, *0.87*	54, 56
Montreal (1995-2019)	y=0.99*x	y=1.04*x	*0.34*, **44**	*0.32*, **42**	*0.34*, **39**	*0.90*, *0.85*	*0.91*, *0.86*	*0.87*, *0.82*	**47, 52**
Quebec (1996-2019)	y=0.98*x	y=1.02*x	0.44, 51	0.39, 45	0.46, 46	*0.97*, *0.97*	*0.97*, *0.98*	*0.95*, *0.95*	47, 52
Toronto (2004-2019)	y=1.02*x	y=1.04*x	*0.67*, **40**	*0.64*, **39**	*0.74*, **37**	*0.96*, *0.96*	*0.97*, *0.98*	*0.94*, *0.94*	**52, 52**
Hamilton (1996-2019)	y=1.00*x	y=1.02*x	*0.53*, **42**	*0.55*, **44**	*0.54*, **42**	*0.95*, *0.97*	*0.95*, *0.96*	*0.92*, *0.93*	**58, 57**
Winnipeg (1984-2018)	y=0.99*x	y=1.00*x	0.37, 57	0.34, 57	0.34, 50	*0.90*, *0.93*	*0.91*, *0.94*	*0.85*, *0.89*	43, 43[#]
Edmonton (1994-2019)	y=1.02*x	y=1.00*x	0.45, 41	0.47, 40	0.53, 45	*0.57*, *0.73*	*0.54*, *0.73*	*0.63*, *0.73*	10, 29
Calgary (1986-2007)	y=1.00*x	y=1.01*x	0.60, 31	0.60, 32	0.61, 33	/	/	/	***-11*, *-5*[#]**
Vancouver (1986-2019)	y=1.00*x	y=1.01*x	0.36, 49	0.36, 47	0.37, 49	0.63, 0.75	0.63, 0.74	0.54, 0.66	23, 27[##]
Victoria (1993-2019)	y=1.01*x	y=1.02*x	0.31, 0.49	0.31, 0.45	0.31, 0.51	0.58, 0.69	0.58, 0.69	0.54, 0.65	23, 33[##]

Table 2. Regression of (BRTs and RF) deweathered against original annual average $PM_{2.5}$ mass concentrations, annual decreasing rate (μg m^{-3} $year^{-1}$) and overall decrease (μg m^{-3}) of deweathered and original $PM_{2.5}$ mass concentrations, and percentage decreases (%) of the provincial total $PM_{2.5}$ emissions in ten Canadian cities during the last decades (decreasing trends were obtained with $P<0.05$ except those marked with "/" for which $P>0.05$; and bold font numbers represent cases with increasing trends).

City	Regression of deweathered against original mixing ratio ($P<0.01$)		Annual decreasing rate (μg m^{-3} $year^{-1}$) and overall decrease (μg m^{-3})			Decreasing percentage (%) of provincial total $PM_{2.5}$ emissions
	BRTs	RF	BRTs	RF	original	
Halifax (2008-2018)	y=1.00*x	y=1.02*x	/	/	/	27
Montreal (2005-2019)	y=1.00*x	y=1.01*x	0.24, 2	0.22, 2	0.25, 2	/
Quebec (1998-2019)	y=1.00*x	y=1.01*x	/	/	/	/
Toronto (2000-2019)	y=1.00*x	y=1.01*x	0.11, 2	0.10, 2	/	/
Hamilton (1998-2019)	y=1.00*x	y=1.01*x	0.15, 4	0.14, 3	0.15, 3	/
Winnipeg (2001-2018)	y=1.04*x	y=1.04*x	**-0.10, -2**	**-0.10, -2**	**-0.09, -1**	**-11**
Edmonton (1998-2019)	y=1.01*x	y=1.03*x	/	/	/	**-40**
Calgary (1998-2014)	y=1.00*x	y=1.03*x	/	/	/	**-38**
Vancouver (2004-2019)	y=0.99*x	y=1.02*x	/	**-0.08, -1**	/	28
Victoria (1999-2019)	y=1.00*x	y=1.03*x	/	**-0.08, -1**	**-0.07, -1**	42

Table 3. Trends in deweathered and original annual average O_3 and O_x mixing ratios at levels below and above 40 ppb in ten Canadian cities during the last decades ([#]decreasing tends with $P<0.05$; [##]no trend or stable trend with $P>0.10$; [###]increasing trend with $P<0.05$).

	O_3						O_x					
	≥ 40 ppb			< 40 ppb			≥ 40 ppb			< 40 ppb		
	BRTs	RF	Original	BRTs	RF	Original	BRTs	RF	Original	BRTs	RF	Original
Halifax (2000-2017)	↓[#]	↓	↓	/[##]	/	/	↓	↓	↓	↓	↓	↓
Montreal (1997-2010)	↓	↓	↓	↑[###]	↑	↑	↓	↓	↓	/	/	/
Quebec (1995-2019)	↓	↓	↓	↑	↑	↑	↓	↓	↓	/	↓	/
Toronto (2003-2019)	↓	↓	↓	↑	↑	↑	↓	↓	↓	↓	↓	↓
Hamilton (1996-2019)	↓	↓	↓	↑	↑	↑	↓	↓	↓	/	/	/
Winnipeg (1985-2018)	↓	/	↓	↑	↑	↑	↓	↓	↓	↓	↓	/
Edmonton (1981-2019)	/	/	/	↑	↑	↑	↓	↓	↓	↓	↓	↓
Calgary (1986-2014)	/	/	↓	↑	↑	↑	↓	↓	↓	↓	↓	↓
Vancouver (1986-2019)	↓	↓	↓	↑	↑	↑	↓	↓	↓	↓	↓	↓
Victoria (1999-2019)	↓	↓	↓	↑	↑	↑	↓	↓	↓	/	/	/

Fig. 1. Performance evaluation of the predicted NO_2 hourly mixing ratios by BRTs and RF algorithm against those observed in Halifax during 1996-2017. Red lines represent linear regression, and color bar reflects data number density. Note that different observational data sets are shown between (a) and (b) because the inputs for the two packages (BRTs and RF) are randomly divided into two groups for training and testing.

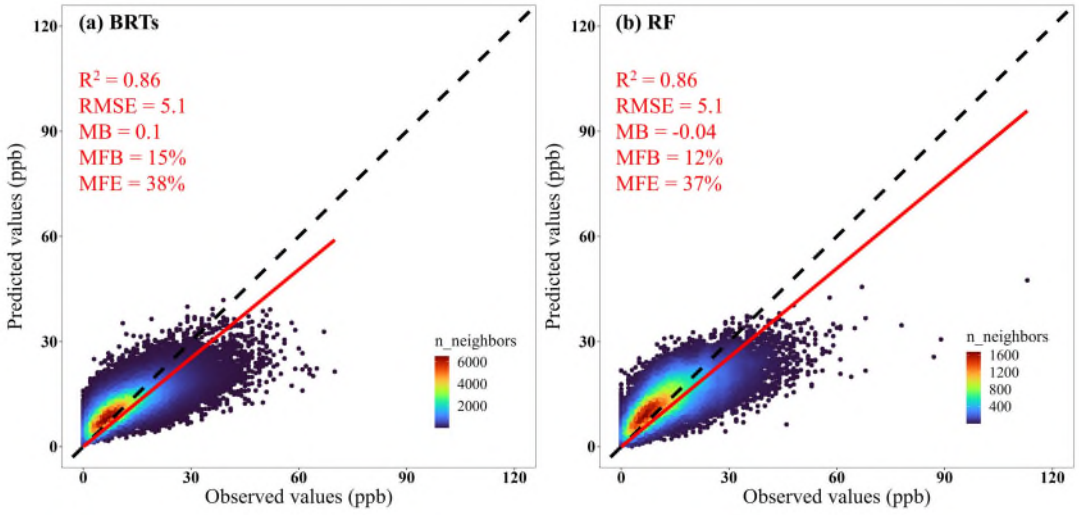

Fig. 2. Correlations between hourly $PM_{2.5}$ concentration in a single year and 22-year average $PM_{2.5}$ concentration in each hour of the year in Edmonton. Left columns show percentile series of $PM_{2.5}$ in 1998, 1999 and 2019, respectively, against the corresponding 22-year average series. Right column shows time series of $PM_{2.5}$ in 1998, 1999 and 2019, respectively, against the corresponding 22-year average series. Red straight and dash lines in a, c and e represent the regression curves within linear ranges and their extensions out of the ranges; vertical arrows represent the distance of the predicted values from the regression curve. Red straight lines and black dash lines in b, d and f represent the regression curves and 1:1 lines, respectively.

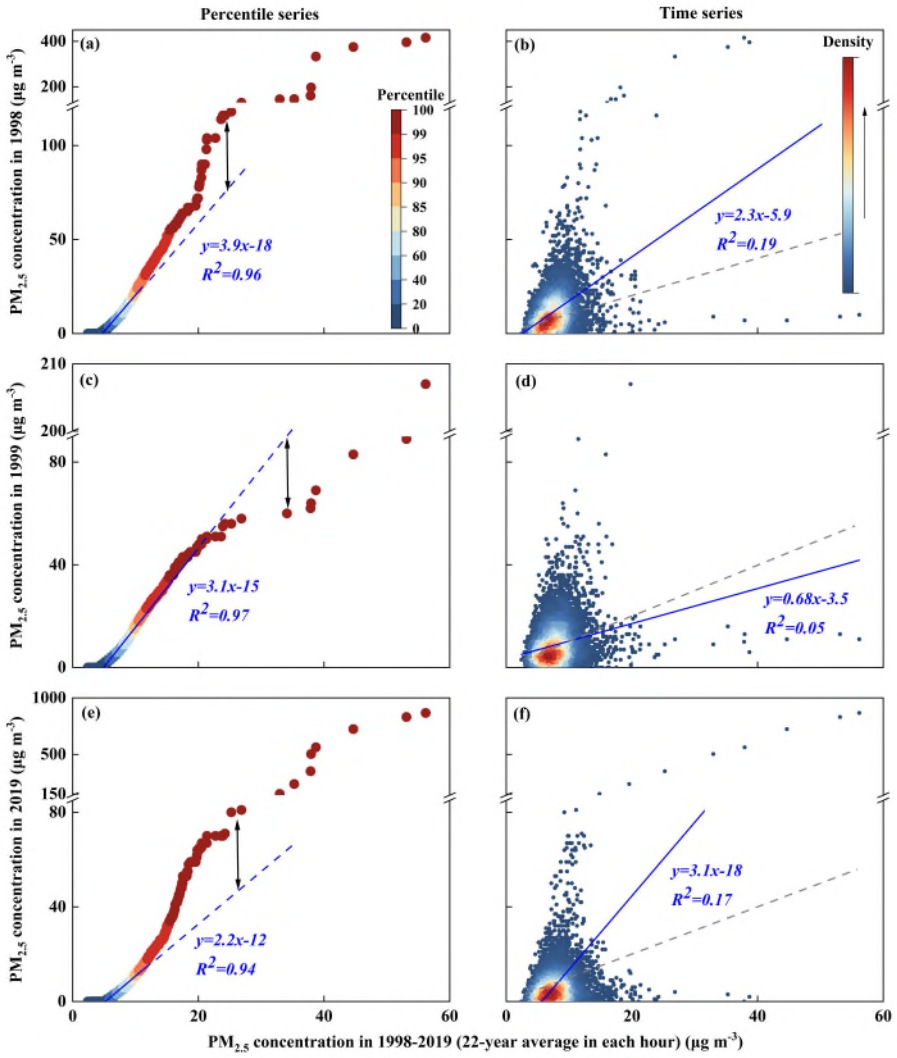

Fig. 3. Trends of original annual average NO_2 and $PM_{2.5}$ in five eastern (upper row) and five western (lower row) Canadian Cities.

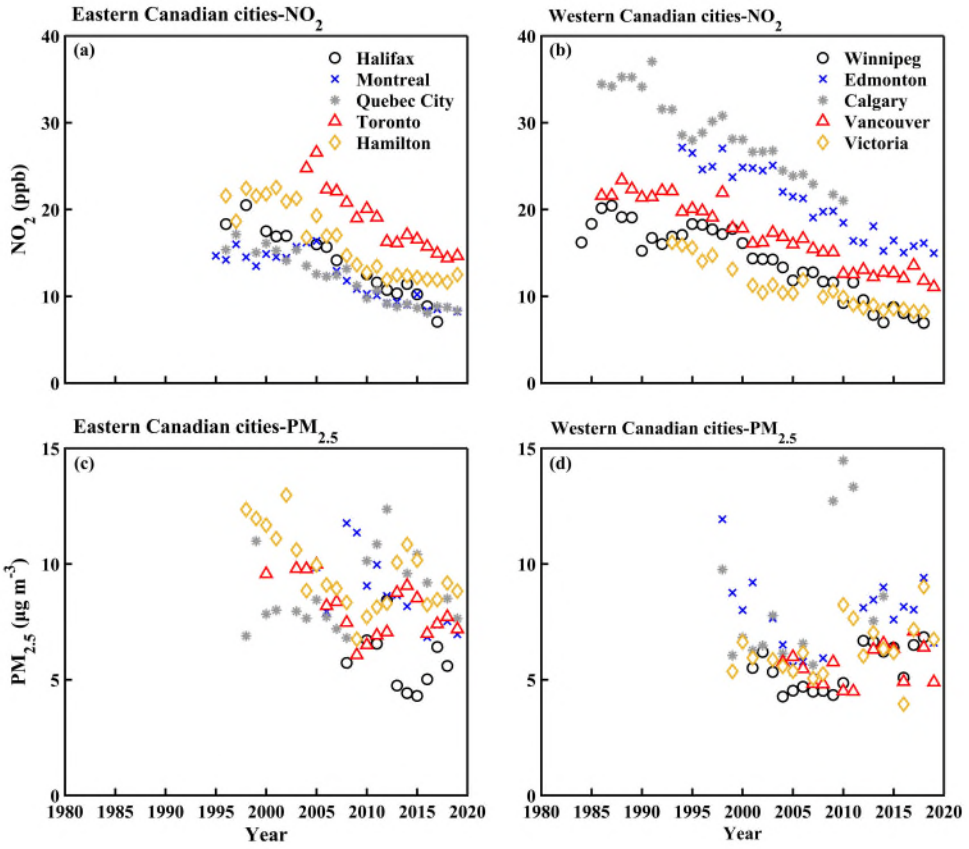

Fig. 4 Deweathered hourly mixing ratios of O_3 (left column) and O_x (right column) at levels ≥40 ppb in five eastern Canadian cities.

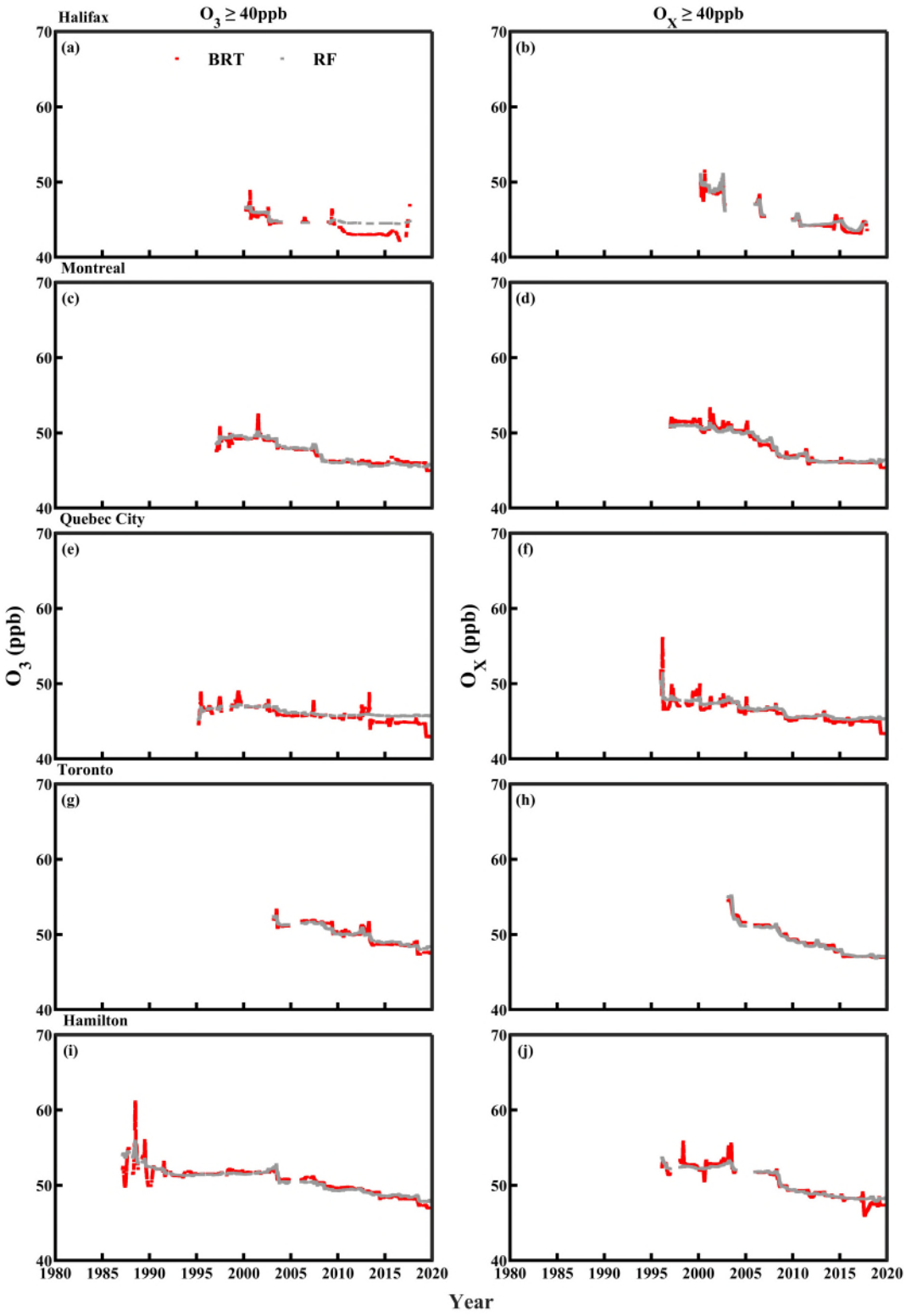

Fig. 5. The calculated perturbation contribution to the corresponding original annual average $PM_{2.5}$ concentration (left column) and the mean and standard derivation of the calculated perturbation (right column) in five western Canadian cities.